RF CAD-Assisted Nonlinear Transmission Line Model of Distributed Passive Intermodulation

RF CAD-Assisted Nonlinear Transmission Line Model of Distributed Passive Intermodulation

Alexey Shitvov[(1)], Dmitry Kozlov[(1)], Alexander Schuchinsky[(2)]

[(1)] *The Institute of Electronics, Communications and Information Theory (ECIT), Queen's University Belfast*
Queen's Road, Belfast, BT3 9DT, United Kingdom
Email: a.shitvov@qub.ac.uk

[(2)]*Department of Electrical Engineering & Electronics of the University of Liverpool*
Email: A.Schuchinsky@liverpool.ac.uk

INTRODUCTION

With the rapid proliferation of high data rate mobile wireless and high-throughput satellite communications and advances of the next generation smart multi-radio base-stations and user terminals, the hardware integration and dynamical reconfigurability become ever more important in view of the commercial feasibility of complex transceiver architectures. Planar microwave technologies provide essential flexibility and reasonable cost for design of complex passive components and system integration. Modern RF and microwave laminate materials enable high-performance distributed circuits and multi-layer integration that suit a wide range of communication frequencies, from legacy sub-6 GHz through 60 GHz and beyond, for a number of general-purpose commercial and mission critical applications. Although the state-of-the-art RF laminate materials feature low loss, negligible dielectric dispersion, excellent thermal and mechanical properties, as well as tight fabrication tolerances and relatively low cost, the microwave circuit processing often causes conspicuous deviations of the component performance. This particularly concerns the linearity of passive distributed microwave circuits exposed to high-power multi-carrier analog and digital signals in filters, phase-shifters and multiplexers in frequency division duplex (FDD) base-station antennas and other passive devices.

The frequency response of passive microwave circuits operated with high-power RF signals at ambient temperatures frequently contains harmonics and intermodulation (IM) products of the carriers, also known as passive intermodulation (PIM). When the IM products are present at the receiver input they raise the receiver noise, thereby causing significant distortion of the communication signals and a range detection error of the radars. It is known that when the power of propagating signals is relatively high, the dielectric and conductor materials exhibit weakly nonlinear response. Additionally, the current-voltage characteristic of electrical contacts also becomes nonlinear, e.g., due to the tunnelling current [1] and constriction resistance [2]. The nonlinearities in passive RF components typically have distributed nature and may be caused by several concurrent physical phenomena. Thus, an accurate modelling of distributed PIM generation requires a credible theoretical framework that extends beyond the capabilities of the basic nonlinear transmission line (TL) analyses commonly used in previous studies.

In this paper, two approaches to physical modelling and characterisation of PIM generation in transmission lines with weak distributed nonlinearities (TLDN) are presented. An analytical model for the analysis of TLDNs is proposed, which allows accurate prediction of the forward (i.e., measured at the output terminal) and reverse (i.e., measured at the circuit input terminal and also known as reflected) PIM products in uniform microstrip lines of finite length, taking into account multiple nonlinear sources. The numerical implementation of the proposed model with a commercial Harmonic Balance (HB) solver is next discussed in details. It is shown that the phenomenological parameters of the equivalent circuit models of uniform transmission lines and microstrip discontinuities, which include nonlinear lumped elements described by ordinary analytical or compact non-analytical modulus-type polynomial models, can be retrieved from the conventional two-tone PIM test and used for accurate modelling of forward and reverse PIM products generated by distributed nonlinearities in microwave circuits. The proposed cascaded nonlinear circuit model enables taking into account the effects of a complex circuit layout and arbitrary signal waveforms.

MECHANISMS AND SOURCES OF INTRINSIC NONLINEARITY IN PLANAR MICROWAVE CIRCUITS

Since the report [3], which represents one of the most comprehensive compendiums of different physical phenomena that can cause PIM generation in microwave circuits, a number of studies have been carried out in order to develop a practical means of modelling, characterisation and mitigation of the nonlinear distortions in hollow metallic waveguides and planar microwave components commonly utilized in mobile wireless base station antennas and satellite payloads. Three distinct types of the PIM effects in passive microwave circuits have received considerable attention in academia and industry.

The contact PIM phenomena have been extensively studies in the context of design of quality waveguide flanges [4] and self-deployable wire mesh reflectors [5], wherein the tunnelling current and constriction resistance were identified as the principal mechanisms of electrical nonlinearity. The studies on characterisation of soldered joins in printed circuit boards (PCB) by PIM measurements also revealed important factors related to the joint internal structure and chemical composition. The second group of PIM studies concerned the electro-thermal effects, particularly those due to the temperature dependent volume resistivity, [6-7]. The electro-thermal IM proved to be a dynamical nonlinear effect, whereby the IM products appear as the result of carrier modulation by a low-frequency thermal dynamics through a thermal feedback. It has been observed that the electro-thermal PIM exhibits discernible level with the frequency roll-off 10 dB per decade of the carriers' offset. Therefore it is particularly notable when the carriers are close to each other, i.e., at frequency separation from 1 Hz to few kHz, which is practically undetectable with the commercial PIM analyzers. The third type of PIM is due to the distributed nonlinearities in commercial PCB components associated with the intrinsic properties of the constituent conductor and dielectric materials, conductor interface and edge, as well as fabrication processes. This PIM in PCB circuits is manifested by the carriers separated for more than 200 kHz, in contrast to the electro-thermal PIM. Although the understanding of the physical origins of the PCB nonlinearities and a means of their mitigation is still open research topic, some recently published insightful trends and observations warrant further effort in developing the theoretical models and efficient CAD tools.

The distributed nature of microstrip nonlinearities has been previously confirmed by extensive experimental studies and simulations [8]. It has been found that the distributed nonlinearity of commercial laminate materials can be described by either voltage-dependent p.u.l. capacitance or current-dependent p.u.l. resistance, i.e., associated with the dielectric substrate or signal conductor, respectively. The former nonlinearity is mainly observed in PCB laminates which are not qualified for the base station antenna and high power applications. The conductor type nonlinearity is usually weak and typically associated with the signal track etching and finishing, rather than the cladding material itself, which nowadays is a fine grain very low profile (VLP) electrodeposited (ED) copper in almost all high-performance microwave laminates. The two-tone PIM measurements using commercial PIM analyzers typically show that neither the conductor nor the substrate PIM levels depend on the carriers' separation in a range from 200 kHz to 25 MHz, which suggests negligible contribution from the electro-thermal nonlinearity and circuit dynamics in the tests.

To give some insight in the typical PIM sources, Fig. 1(a) shows the results of the two-tone PIM measurements on identical microstrip layouts fabricated on two different PCB laminate materials. In Fig. 1, both materials are from the same manufacturer and both are PTFE/ceramic based woven glass laminates with the same 1 oz. VLP ED copper. Both laminates have the dielectric constant of 3.5 and similar dissipation factors. 'Laminate A' material is not qualified for base station antenna applications, whereas 'Laminate B' material is a low-PIM substrate. The track etching and a 1 um immersion tin finishing on both laminates were performed by the same PCB processing workshop in one batch. The test layout consists of two tapered and one uniform microstrip lines of the same total length but different width of the signal tracks, Fig. 1(a). When the PCBs arrived they were measured using a commercial two-tone PIM analyzer for the forward (i.e., at the line output) third-order PIM (PIM3) at E-GSM 900 frequency $f_{IM3} = 2f_1 - f_2 = 910$ MHz ($f_1 = 935$ MHz and $f_2 = 960$ MHz) and at PCS 1900 frequency $f_{IM3} = 1870$ MHz ($f_1 = 1930$ MHz and $f_2 = 1990$ MHz) using two 40 dBm CW carriers. The PIM levels on both materials show distinctive decrease as the signal track width increases, whereas the absolute level of the PIM products on Laminate A remains much higher. The PCB microscopy shown in Fig. 1(c) suggests that the PIM sources in the microstrip lines on Laminate A can be attributed to the "black tin" contamination at the track edges, which is unevenly distributed along the strip.

To illustrate the mechanism of the PIM generation, Fig. 1(d) displays the results of the experiment with a localised PIM source emulated by a small (1 mm × 1 mm) pencil mark on a piece of paper. The mark, placed on the top of wide microstrip line fabricated on the low-PIM Laminate B, see Fig. 1, was moved across the strip. The measurements of forward PIM3 products have been made at frequency $f_{IM3} = 910$ MHz and carrier power of 43 dBm. The results shown in Fig. 1(d) demonstrate that strip edges, where the current is bunching, produce PIM3 of substantially higher level. To understand whether the uneven distribution of PIM sources along the microstrip length bears implications for the distributed PIM modelling, the near-field mapping of the PIM3 product was performed along the uniform microstrip line on Laminate A material at frequency $f_{IM3} = 910$ MHz and carrier power 43 dBm. Figure 2(a) shows the measurement results in comparison with the model predictions based on the assumption of evenly distributed nonlinearity. So, one may wonder if the observed discrepancy could be due to random distribution of PIM sources. To clarify this matter, the experiment was set up with a number of lumped PIM sources, each emulated by a pencil mark on a piece of paper that generated ca. −70 dBm forward and reverse PIM3 when placed on top of the signal strip. The pencil marks, ca. 1 mm ×1 mm, were placed one by one at the centre of the signal strip of the low-PIM uniform microstrip line ($W = 3.4$ mm) on Laminate B material, and the near-filed PIM probing was performed for each arrangement of the PIM sources. The measurement and simulation results in

Fig. 2(b) reveal a distinct trend in the formation of the cumulative growth of the PIM products toward the load and troughs toward the line input, cf. [8], as the number of the lumped sources increases. The position and depth of the troughs also depend on the microstrip TL terminations.

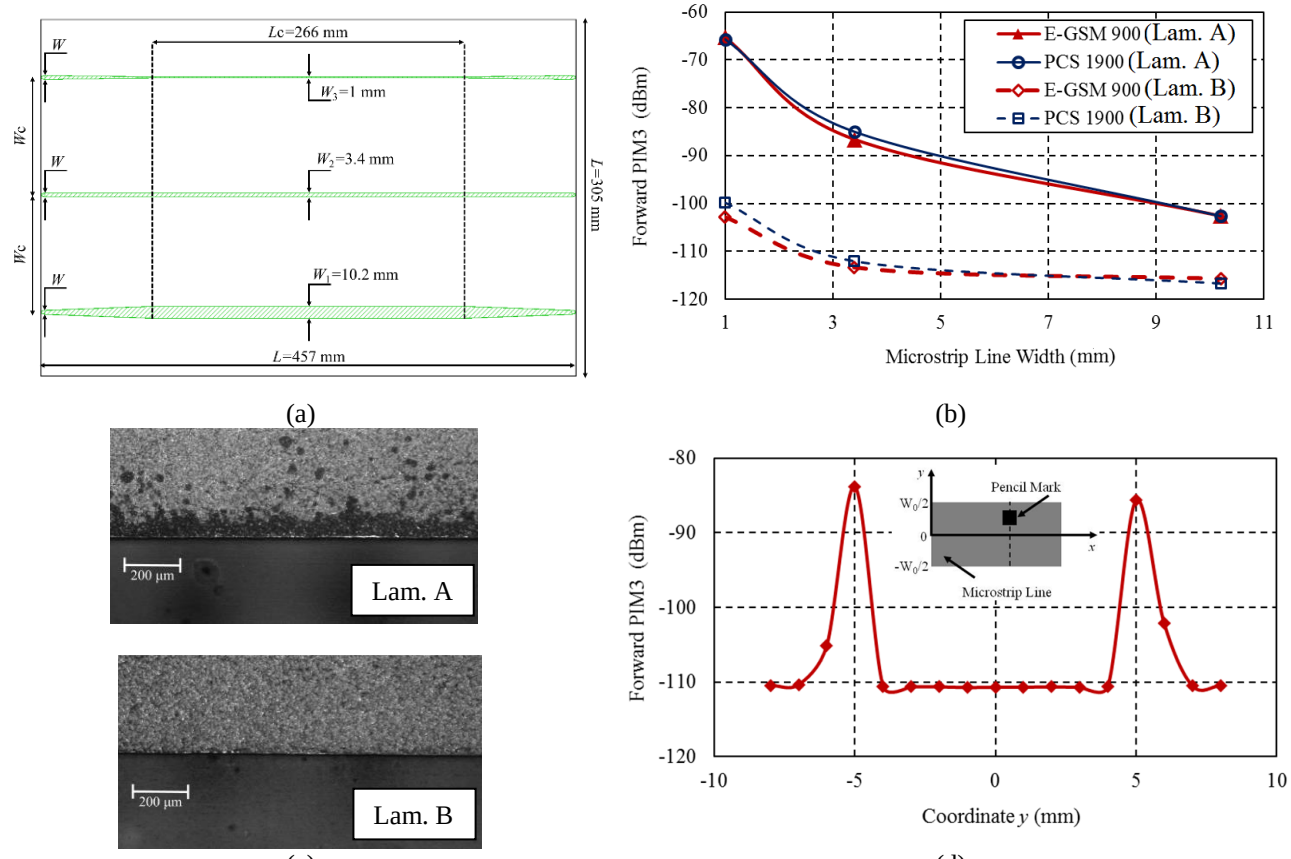

Fig. 1. (a) Test microstrip layout, (b) two-tone forward PIM3 measurements on the test microstrip lines in E-GSM 900 and PCS 1900 bands at 40 dBm carrier power, (c) optical microscopy of the microstrip edge on two laminate materials, and (d) forward PIM3 products of frequency f_{IM3} = 910 MHz on the microstrip line of width W=10.2 mm fabricated on the low-PIM Laminate B material generated by the pencil mark moved across the strip. Carrier power is 43 dBm.

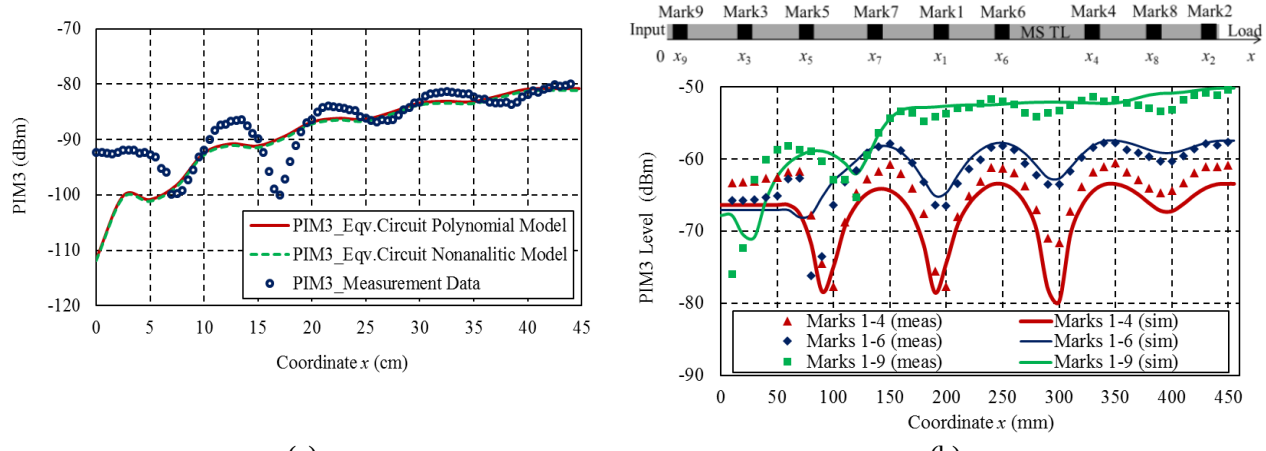

Fig. 2. (a) Near-field mapping and simulations (see the next sections for details) of PIM3 distribution along the uniform strip (W = 3.4 mm) on Laminate A material at f_{IM3} = 910 MHz and carrier power 43 dBm.

Inspection of Fig. 1(b) shows that PIM level in the low-PIM microstrip line on Laminate B very slowly decreases with the strip widths W > 3 mm. Given the residual PIM3 of −125 dBm, we can conclude that the substrate nonlinearity plays

an important role, especially for the wide strips. This suggests the need of developing a distributed model of PIM generation taking into account the concurrent effects of conductor and substrate nonlinearities. An RF CAD implementation of such a model will allow us to assess the combined effects of lumped and distributed PIM sources and possibly locate lumped nonlinearities in distributed circuits.

THEORETICAL MODEL OF DISTRIBUTED PIM IN MICROSTRIP LINES

Based on the observations made in the previous section, we start the theoretical analysis with the nonlinear model of a TLDN unit cell that accounts for both conductor and substrate nonlinearities, following the approach in [8] and [9]. The analysis is based on the local static polynomial model of nonlinearity, which is inherently similar to the high order sinusoidal input describing functions approach. The choice of the memoryless polynomial regression model is justified by our experimental data. Indeed, frequency-sweep measurements of the PIM products of different orders on the test microstrip lines in our study demonstrate constant PIM level across the whole measured band when either carrier sweeps across the Tx band. The PIM level also remains frequency independent when the carrier power varies. Therefore, we assume that the distributed PIM process can be characterised in the framework of the TLDN model with the nonlinear p.u.l. parameters

$$\begin{aligned} L'(I) &= L'_0 + L'_{NL}(I) = L'_0 + \sum\nolimits_{n=1}^{(N-1)/2} L'_{2n} I^{2n}, \quad R'(I) = R'_0 + R'_{NL}(I) = R'_0 + \sum\nolimits_{n=1}^{(N-1)/2} R'_{2n} I^{2n}, \\ C'(V) &= C'_0 + C'_{NL}(V) = C'_0 + \sum\nolimits_{n=1}^{(N-1)/2} C'_{2n} V^{2n}, G'(V) = G'_0 + G'_{NL}(V) = G'_0 + \sum\nolimits_{n=1}^{(N-1)/2} G'_{2n} V^{2n}, \end{aligned} \tag{1}$$

where N is an odd number and the parameters L'_{2n}, R'_{2n}, C'_{2n} and G'_{2n} are essentially phenomenological and subject to experimental retrieval. It is noteworthy that the nonlinear parameters of the TL are described by the polynomials of I^2 and V^2. Validity of such an approximation has been verified by cross-band PIM measurements, where the sum product of the carrier frequencies from the E-GSM 900 band was measured in the PCS 1900 band. The measured level of the 2nd order PIM products was below the equipment noise floor, which suggests the absence of the even-order PIM products and thus justifies the approximations defined in (1). Given the nonlinear model (1), the nonlinear voltage and current waveforms on a uniform TLDN are described by the generalised telegrapher's equations:

$$\frac{\partial I(x,t)}{\partial x} = -C'_0 \frac{\partial V(x,t)}{\partial t} - G'_0 V(x,t) - \frac{\partial I_{NL}(x,t)}{\partial x}, \quad \frac{\partial V(x,t)}{\partial x} = -L'_0 \frac{\partial I(x,t)}{\partial t} - R'_0\, I(x,t) - \frac{\partial V_{NL}(x,t)}{\partial x}. \tag{2}$$

The linear p.u.l. parameters R_0', L_0', C_0' and G_0' can be calculated by a quasi-static analysis and directly related to the microstrip geometry. In fact, equations (2) describe a TLDN with a voltage-controlled current source and a current-controlled voltage source:

$$\frac{\partial I_{NL}(x,t)}{\partial x} = \frac{\partial\left(C'_{NL}(V)V(x,t)\right)}{\partial t} + G'_{NL}(V)V(x,t), \quad \frac{\partial V_{NL}(x,t)}{\partial x} = \frac{\partial\left(L'_{NL}(I)I(x,t)\right)}{\partial t} + R'_{NL}(I)I(x,t). \tag{3}$$

By differentiating the first equation in (2) with respect to x and the second equation with respect to t, after some algebraic manipulations we obtain the following equation for the electric current wave $I(x,t)$ on the TL:

$$\frac{\partial^2 I(x,t)}{\partial x^2} = L'_0 C_0 \frac{\partial^2 I(x,t)}{\partial t^2} + \left(R'_0\, C'_0 + G'_0\, L'_0\right)\frac{\partial I(x,t)}{\partial t} + G'_0\, R'_0\, I(x,t) + C'_0 \frac{\partial^2 V_{NL}(x,t)}{\partial x \partial t} + G'_0 \frac{\partial V_{NL}(x,t)}{\partial x} - \frac{\partial^2 I_{NL}(x,t)}{\partial x^2}. \tag{4}$$

In case when the source signal consists of two carriers with angular frequencies ω_1 and ω_2, the effect of TL nonlinearity will manifest itself in generation of harmonics of the carrier frequencies and intermodulation products. Therefore, propagating current and voltage waveforms can be represented by double complex Fourier series [10, Ch. 5]:

$$\begin{aligned} I(x,t) &= \sum_{m=-\infty}^{\infty}\sum_{n=-\infty}^{\infty} \hat{I}_{mn}(x)\, e^{j\omega_{mn}t}, \qquad I_{NL}(x,t) = \sum_{m=-\infty}^{\infty}\sum_{n=-\infty}^{\infty} \hat{I}_{NL_{mn}}(x) e^{j\omega_{mn}t}, \\ V(x,t) &= \sum_{m=-\infty}^{\infty}\sum_{n=-\infty}^{\infty} \hat{V}_{mn}(x) e^{j\omega_{mn}t}, \qquad V_{NL}(x,t) = \sum_{m=-\infty}^{\infty}\sum_{n=-\infty}^{\infty} \hat{V}_{NL_{mn}}(x) e^{j\omega_{mn}t}, \end{aligned} \tag{5}$$

where $\omega_{mn} = m\omega_1 + n\omega_2$. Substituting (5) into (4) and collecting the terms, the nonlinear voltage and current sources at the specific angular frequency ω_{mn} can be expressed as

$$\frac{d\hat{I}_{NL_{mn}}(x)}{dx} = \sum\nolimits_{l=1}^{(N-1)/2}\left(j\omega_{mn}C'_{2l} + G'_{2l}\right)F_{mn}\left\{V^{2l+1}(x,t)\right\}, \quad \frac{d\hat{V}_{NL_{mn}}(x)}{dx} = \sum\nolimits_{l=1}^{(N-1)/2}\left(j\omega_{mn}L'_{2l} + R'_{2l}\right)F_{mn}\left\{I^{2l+1}(x,t)\right\}, \tag{6}$$

where the operator $F_{mn}\{\ldots\}$ is the complex amplitude of its argument at frequency ω_{mn}. Hence, equation (4) for the complex Fourier amplitudes (5) at frequency ω_{mn} reads:

$$\frac{d^2\hat{I}_{mn}(x)}{dx^2} - \gamma_{mn}^2 \hat{I}_{mn}(x) = \frac{\gamma_{mn}}{Z_{c_{mn}}}\frac{d\hat{V}_{NL_{mn}}(x)}{dx} - \frac{d^2\hat{I}_{NL_{mn}}(x)}{dx^2} \tag{7}$$

where $\gamma_{mn} = \sqrt{\left(R_0' + j\omega_{mn}L_0'\right)\left(G_0' + j\omega_{mn}C_0'\right)} \approx \alpha + j\beta_{mn}$, $Z_{c_{mn}} = \sqrt{\left(R_0' + j\omega_{mn}L_0'\right)/\left(G_0' + j\omega_{mn}C_0'\right)}$. In general, equation (7) is a nonlinear differential equation, since its RHS contains the nonlinear functions of the current and voltage distributions on the transmission line. However, taking into account that passive nonlinearity is weak, (7) can be linearized and solved by substituting the linear (small-signal) solutions for the carrier current and voltage waves into the RHS of (7). The resulting linear system is solved at each IM frequency $\omega_M = 0.5\left[\left(M+1\right)\omega_1 - \left(M-1\right)\omega_2\right]$ for the IM current distribution (note that M is negative for the upper sideband products if $\omega_1 < \omega_2$). The power of the forward and reverse PIM products of M-th order at the output and intput, respectively, of a matched uniform TL of length L is

$$P_{fwd_M}(L) = \frac{1}{2}\mathrm{Re}\left\{Z_{c_M}\right\}\left|A_M\right|^2\left(\left|M\right|-1\right)^2\alpha^2L^2e^{-2\alpha L}, \quad P_{rev_M}(L) = \frac{1}{2}\mathrm{Re}\left\{Z_{c_M}\right\}\frac{\left|A_M\right|^2}{\beta_M{}^2}\left(\left|M\right|-1\right)^2\alpha^2\sin^2\left(\beta_M L\right), \tag{8}$$

where $A_M = \sum_{l=1}^{(N-1)/2}\binom{2l+1}{l+1}\frac{\hat{I}}{Z_0}\left|\hat{I}\right|^{2l}\frac{\gamma_M\left(j\omega_M L_{2l}' + R_{2l}'\right) + \chi_M Z_{c_M}^2\left|Z_{c_M}\right|^{2l}\left(j\omega_M C_{2l}' + G_{2l}'\right)}{2^{2l}\left(\chi_M^2 - \gamma_M^2\right)}\binom{2l+1}{l+1-0.5\left(M+1\right)}$, $\binom{k}{l}$ are the binomial coefficients, $\hat{I}$ is the complex current amplitude at a carrier frequency (equal amplitude carriers) and $\chi_M = \left|M\right|\alpha + 0.5j\left[\left(M+1\right)\beta_1 - \left(M-1\right)\beta_2\right]$. The closed-form equations (8) for the power of the forward and reverse PIM products of arbitrary order M on a matched transmission line with weak distributed nonlinearity and small dispersion have been derived for the general N-th order static polynomial model (1). Consistently with [8], equations (8) shows that power of forward PIM products increases monotonically with the line length while $\alpha L << 1$, and the reverse PIM power has regular undulation as the line length increases and do not vanish even on the matched TL [8]. The effects of non-uniform current and field distributions across microstrip can be easily accommodated in (8) through the corresponding geometrical factors, [11-12]. Equations (8) can, in principle, be directly used to characterise the TL nonlinearity defined by (1). The number of the phenomenological parameters can be reduced, e.g., by considering only the strongest contributions or adopting a different nonlinear model. In the following analysis we assume that the conductor nonlinearity is represented by a current-dependent p.u.l. resistance, due to the negligible kinetic inductance in ordinary conductors. The substrate nonlinearity is given by a voltage-dependent p.u.l. capacitance.

The analysis based on (8) shows that dominant nonlinearities can be identified by comparing the two-tone PIM3 products measured when both carrier frequencies are in either of two different frequency bands, see Fig. 3. The TL models with dominant p.u.l. nonlinear resistance or dominant p.u.l. nonlinear inductance in Fig. 3 correspond to the simplest (N = 3) polynomials in (1). The nonlinear coefficients R'_2 and L'_2 were determined by fitting the simulated two-tone forward PIM3 products of (9) to the values measured at 910 MHz with two 43 dBm CW carriers on the reference Laminate A uniform microstrip line in Fig. 1. The results in Fig. 3 show noticeable increase of the forward PIM3 with frequency in the case of inductive nonlinearity and no changes in the case of resistive nonlinearity, which theoretically confirms the previous conjecture on negligible effect of inductive nonlinearity deduced from the measurements in Fig. 1(b).

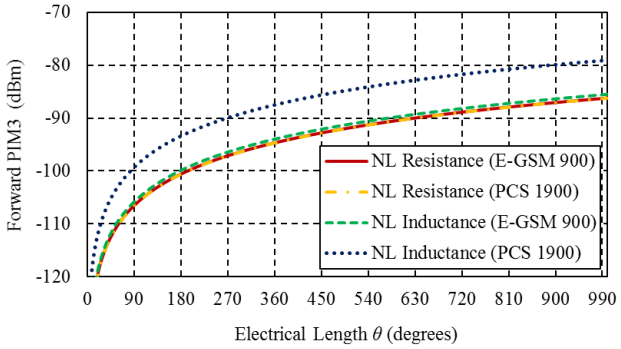

Fig. 3. Theoretical analysis of the forward third-order PIM product versus the transmission line length with dominant nonlinear p.u.l. resistance or inductance, when the carrier frequencies are in either E-GSM 900 or PCS 1900 bands.

RF CAD ASSISTED NONLINEAR CHARACTERISATION OF MICROSTRIP CIRCUITS

Although equations (9) are instrumental for understanding the basic trends and dependencies in distributed PIM generation, their practical implementation is hampered by several factors. Firstly, the derived equations describe the PIM generation by travelling waves on matched uniform transmission line. Indeed, equations (9) can be, in principle, extended

to include the effects of the source and load impedances, yet their complexity will increase accordingly. Moreover, any practical microstrip circuit has a complex layout comprising of multiple sections of uniform transmission lines of different length and width, various microstrip discontinuities, coupled lines, resonators and possibly multiple input and output ports. This necessitates the development of a more efficient approach based on the commercial RF CAD methods and tools. However, the retrieval of the nonlinear parameters, which are characteristic of the conductor and substrate materials and fabrication, is still more convenient to conduct using some basic microstrip layouts.

The CAD implementation of a short (i.e., considerably smaller than the characteristic wavelength) section of TLDN is shown in Fig. 4(a), where the TL section of a length l_0 is represented by a symmetrical lumped-element T-network. Indeed, the transfer matrices of a TL section and T-network have similar structure, so that the equivalent circuit parameters can be easily obtained in a low-loss approximation: $L_0 \approx Z_c(1-\cos\theta_0)/(2\omega\sin\theta_0)$ and $C_0 \approx \sin\theta_0/(\omega Z_c)$, where $\theta_0 = \beta l_0$. The results in Fig. 4(b) confirm that partitioning the test TL length in 5° subsections modelled by the equivalent T-networks provides reasonable matching up to the third harmonic of the characteristic frequency of 910 MHz. The small-signal TL losses can be added empirically by fitting to the small-signal S-parameters. After that the analysis extends to the large-signal model, where the lumped resistors and capacitors are approximated by corresponding polynomials (1) whose coefficient are extracted by fitting to the PIM3 measurement data.

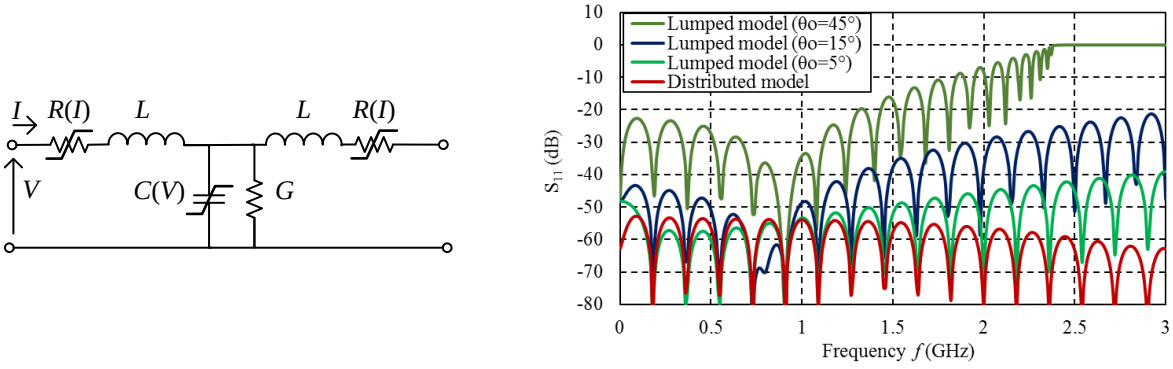

(a) (b)

Fig. 4. (a) CAD implementation of a short length of uniform transmission line with distributed nonlinearity and (b) simulation of the small-signal reflection scattering on a matched lossless TL of the electrical length 900° (at 910 MHz).

To validate the proposed approach, the model in Fig. 4(a) has been implemented in Keysight ADS software and the nonlinear simulations of the forward and reverse PIM products have been carried out with the Harmonic Balance (HB) solver. To improve the numerical accuracy, short 5° cells were combined to form a longer 45° cell. The 45° cell was characterised by the X-parameters. The complete TL length was simulated as a nonlinear cascaded network of 45° cells with the pre-defined X-parameters.

The nonlinear parameters of the equivalent circuit resistor of the 5° T-cell, have been extracted by fitting to the forward PIM3 products measured on the reference uniform microstrip line on Laminate A material in Fig. 1(a) in a range of the carrier power varied from 30 to 44 dBm, whereas the dielectric substrate was assumed linear. Taking advantage of the ADS HB capability of working with user defined nonlinear models, two different polynomials have been compared, viz., the analytical polynomial, $R(I) = R_0 + \sum_{n=1}^{(N-1)/2} R_{2n} I^{2n}$, and the modulus polynomial, $R(I) = R_0 + \sum_{n=1}^{N} R_n |I|^n$. It is noteworthy that both polynomials do not produce even-order IM terms and harmonics. It appeared that the root mean squared deviation (RMSD) decreases as the polynomial order increases, and it achieves a residual error when the polynomial order is least $N = 9$ for the analytical polynomial, whereas $N = 3$ was sufficient for the modulus polynomial. The residual error of 1.5% in both cases is attributed to the PIM measurement uncertainties. The resulting polynomial coefficients are shown in Table 1. Given that the polynomial coefficients were extracted by fitting to the measured forward PIM3 products in the specified power range on the uniform microstrip line. Adequacy of the retrieved models has been verified in the analysis of the reverse PIM3 and high-order PIM products, dependence on the microstrip width, as well as PIM products at power of one carrier varying independently of the other carrier. In Fig. 5(a) and (b), the PIM3 products on the reference uniform microstrip line have been measured and simulated with the varying carrier power P_1, while the carrier power P_2 was fixed. The results show that the modulus polynomial model better approximates the test results than the analytical polynomial.

Table 1. Extracted resistive nonlinearity parameters for the uniform microstrip line on Laminate A in Fig. 1.

n	R_n (Ohm/A^n)	
	Analytical Polynomial $R(I) = R_0 + \sum_{n=1}^{(N-1)/2} R_{2n} I^{2n}$	Modulus Polynomial $R(I) = R_0 + \sum_{n=1}^{N} R_n \lvert I \rvert^n$
0	0.01178	0.01178
1	2.81659×10^{-6}	1.27621×10^{-6}
2	-9.61792×10^{-7}	6.039×10^{-7}
3	1.77514×10^{-7}	0
4	-9.98443×10^{-9}	0

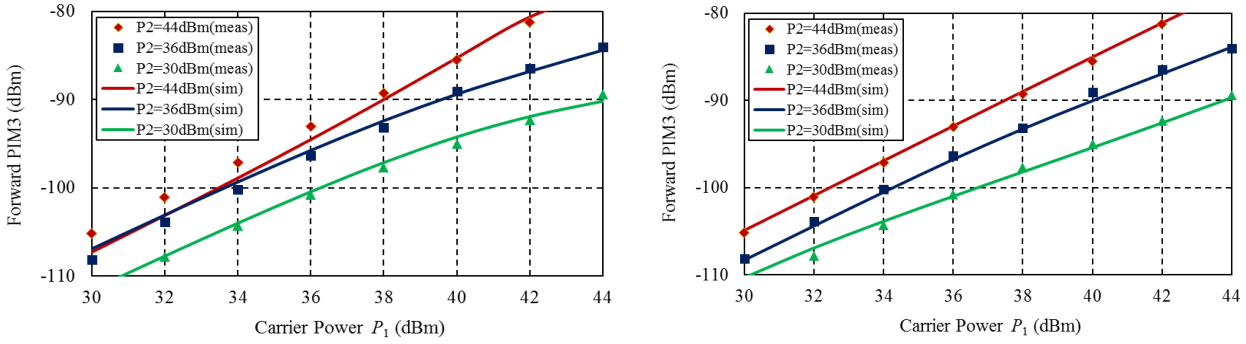

Fig. 5. Simulations vs. measurements of the forward PIM3 product at 910 MHz, as the carrier power P_1 changes while the power P_2 is fixed, using (a) analytical and (b) modulus polynomial models.

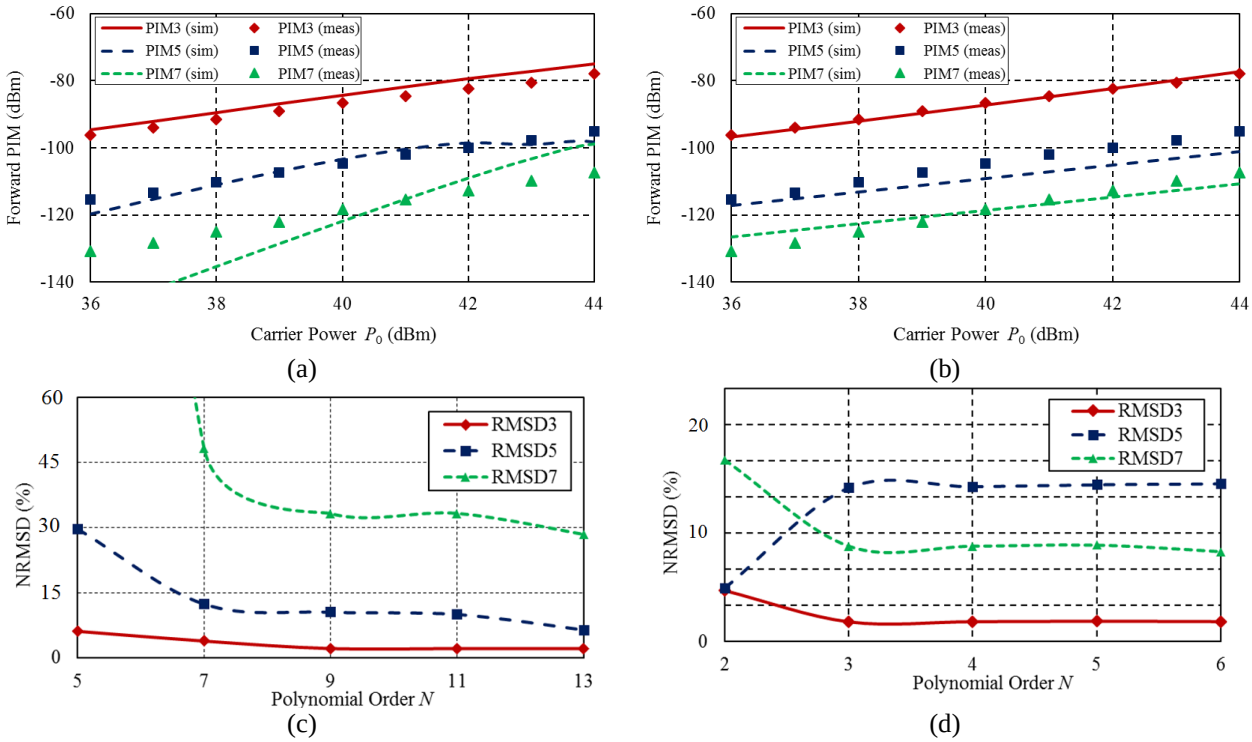

Fig. 6. Simulations vs. measurements of the high-order PIM products vs. carrier power P_0 using (a) analytical and (b) modulus polynomial models, and NRMSD using (a) analytical and (b) modulus polynomial models in Table 1.

Also in Fig. 6(a) and (b) the measurement results for the 5th-order and 7th-order PIM products are juxtaposed with the respective simulation results based upon the coefficients extracted from the PIM3 measurements (see Table 1). The

modulus polynomial again provides better prediction of the high-order PIM products. The RMSD convergence for both polynomial models of different PIM products is shown in Fig. 6(c) and (d). Actually, our simulations suggest that the quality of the analytical model can be further improved by increasing the polynomial degree, so at $N = 23$ the analytical polynomial demonstrates the RSMD for all PIM products similar to the modulus polynomial of order $N = 3$. These observations suggest that the modulus type polynomial model better fits with the experimental data and thus suits well for the CAD assisted characterisation and modelling of distributed PIM generation in planar microwave circuits.

CONCLUSIONS

Characterisation and modelling of distributed passive intermodulation generation in planar microwave components is hampered by a priori unknown physics and location of the sources of microstrip nonlinearities. It has been shown that using even the basic two-tone PIM3 measurements in different frequency bands and in the near-field PIM probing mode on simple microstrip layouts allows identification of the dominant type of the microstrip nonlinearity and PIM generation mechanisms. Using the transmission line formulation and simple static polynomial models of the p.u.l. parameters, the set of general closed-form equations for the forward and reverse PIM products of arbitrary order can be derived from the analysis of the waves propagating on a weakly nonlinear transmission line. It has been shown that an accurate distributed model of PIM generation can be constructed with the aid of Keysight's X-parameter methodology by cascading equivalent-circuit unit cells representing short sections of the nonlinear TL of the electrical length much smaller than the characteristic wavelength. The CAD implementation of the TLDN model allows efficient characterisation of the nonlinear models based on different polynomial approximations of the distributed nonlinearities. It has been demonstrated that the proposed modulus polynomial model provides fairly accurate approximation with only a few terms, whereas the conventional analytical polynomial model requires much higher order of the describing polynomial. The results of the presented analysis can be used for the modelling of PIM generation by arbitrary modulated signals in complex planar microwave circuits and design of low-PIM microwave circuits.

ACKNOWLEDGEMENTS

This work has been carried out in the framework of Marie Curie European Industrial Doctorate (EID) programme ARTISAN jointly with Bell Labs Ireland, grant No. 316426. The authors wish to thank Mr Christian Entsfellner and staff at Rosenberger Hochfrequenztechnik GmbH & Co. KG for support with the key measurement facilities and Dr Efstratios Doumanis for very fruitful discussions of the filter design and characterisation.

REFERENCES

[1] R. Kwiatkowski, et al. "Tunnel conduction consequences in high frequency microcontacts: passive intermodulation effect," *50th IEEE Holm Conf. on Electrical Contacts / 22nd Int. Conf. on Electrical Contacts*, pp. 152 – 159, 2004.

[2] I. Minowa, "A consideration for the non-linear resistance caused by constriction current through two dimensional bridge on a copper printed circuit board," *IEICE Trans. Electron.*, E90-C(7), 1417-1420, 2007.

[3] G.H. Stauss, "Intrinsic sources of IM generation," NRL Memorandum Report 4233, Ch. 5, Naval Research Laboratory Washington D.C., 1980, pp. 65 – 82.

[4] C. Vicente and H. Hartnagel, "Passive-intermodulation analysis between rough rectangular waveguide flanges," IEEE Trans. MTT, vol. 53, no. 8, pp. 2515 – 2525, 2005.

[5] Jie Jianga, et al., "A nonlinear equivalent circuit method for analysis of passive intermodulation of mesh reflectors," *Chinese Journal of Aeronautics*, vol. 27, no. 4, pp. 924–929, 2014.

[6] J.Z. Wilcox and P. Molmud, "Thermal heating contribution to intermodulation fields in coaxial waveguides," *IEEE Trans. Comm.*, vol. 24, no. 2, pp. 238 – 243, 1976.

[7] J.R. Wilkerson, et al., "Electro-thermal theory of intermodulation distortion in lossy microwave components," *IEEE Trans. MTT*, vol. 56, no. 12, pp. 2717 – 2725, 2008.

[8] D. E. Zelenchuk, et al. "Passive intermodulation in finite lengths of printed microstrip lines," *IEEE Trans. MTT*, vol. 56, no. 11, pp. 2426-2434, 2008.

[9] J. Mateu,et al., "Third-Order Intermodulation Distortion and Harmonic Generation in Mismatched Weakly Nonlinear Transmission Lines," *IEEE Trans. MTT*, vol. 57, no. 1, pp. 10-18, 2009.

[10] A. Gelb, W. Vander Velde, *Multiple-Input Describing Functions and Nonlinear System Design*, McGraw-Hill, 1968.

[11] D. Kozlov, "Behavioural and Physical Modelling and Characterisation of Passive Intermodulation," Ph.D. dissertation, Queen's University Belfast, Belfast, United Kingdom, December 2016.

[12] A. Shitvov, et al., "On optimum design of planar microwave components under linearity constraints," *Proc. MULCOPIM 2017*, ESA/ESTEC Noordwijk, The Netherlands, 5-7 April 2017, (accepted).